◆ Human Brain Mapping 37:4581–4596 (2016) ◆

Early Changes of Brain Connectivity in Primary Open Angle Glaucoma

Paolo Frezzotti, Antonio Giorgio,* Francesca Toto, Alessandro De Leucio, and Nicola De Stefano*

Department of Medicine, Surgery and Neuroscience, University of Siena, Siena, Italy

Abstract: Our aim was to assess in primary open angle glaucoma (POAG), a major cause of irreversible blindness worldwide, whether diffuse brain changes recently shown in advanced stage can be detected since the early stage. We used multimodal magnetic resonance imaging (MRI) in 57 patients with the three POAG stages and in 29 age-matched normal controls (NC). Voxelwise statistics was performed with nonparametric permutation testing. Compared with NC, disrupted anatomical connectivity (AC) was found in the whole POAG group along the visual pathway and in nonvisual white matter tracts ($P < 0.001$). Moreover, POAG patients showed decreased functional connectivity (FC) in the visual ($P = 0.004$) and working memory ($P < 0.001$) networks whereas an increase occurred in the default mode ($P = 0.002$) and subcortical ($P < 0.001$) networks. Altered AC and FC were already present in early POAG ($n = 14$) in both visual and nonvisual systems ($P \leq 0.01$). Only severe POAG ($n = 30$) showed gray matter atrophy and this mapped on visual cortex ($P < 0.001$) and hippocampus ($P < 0.001$). Increasing POAG stage was associated with worsening AC in both visual and nonvisual pathway ($P < 0.001$), progressive atrophy in the hippocampus and frontal cortex ($P < 0.003$). Most of the structural and functional alterations within and outside the visual system showed correlation ($P < 0.001$ to 0.02) with computerized visual field and retinal nerve fiber layer thickness. In conclusion, the complex pathogenesis of POAG includes widespread damage of AC and altered FC within and beyond the visual system since the early disease stage. The association of brain MRI changes with measures of visual severity emphasizes the clinical relevance of our findings. *Hum Brain Mapp 37:4581–4596, 2016.*

Key words: glaucoma; magnetic resonance imaging; functional magnetic resonance imaging; atrophy; DTI; connectivity; neurodegeneration; Alzheimer disease

INTRODUCTION

Glaucoma is a major cause of blindness worldwide. A key role in the pathogenesis of this disorder is attributed to the degeneration of the retinal ganglion cells, which progressively leads to visual field damage and, without an appropriate therapy, to a bilateral and irreversible blindness [EuropeanGlaucomaSociety, 2008]. The damage to the axonal projections of retinal ganglion cells is reflected by a thinning of the retinal nerve fiber layer (RNFL) of the optic nerve, which can be assessed noninvasively through optical coherence tomography (OCT) [Bussel et al., 2014]. Thinning of the RGC axons has been linked to a number of neurodegenerative conditions such as Alzheimer disease, Parkinson disease and multiple sclerosis [Calabresi

Contract grant sponsor: Istituto per la Ricerca, la Formazione e la Riabilitazione (I. Ri. Fo. R. onlus).

P.F. and A.G. contributed equally to this work.

*Correspondence to: Nicola De Stefano, MD, PhD, Professor of Neurology, Department of Medicine, Surgery and Neuroscience, University of Siena, Viale Bracci 2, 53100 Siena. E-mail: destefano@unisi.it or Antonio Giorgio, MD, PhD, Department of Medicine, Surgery and Neuroscience, University of Siena, Viale Bracci 2, 53100 Siena. E-mail: giorgio3@unisi.it

Received for publication 5 April 2016; Revised 18 July 2016; Accepted 19 July 2016.

DOI: 10.1002/hbm.23330

Published online 9 August 2016 in Wiley Online Library (wileyonlinelibrary.com).

TABLE I. Clinical-demographic characteristics of the POAG group

Clinical-demographic characteristics	POAG patients
Age, mean ± SD (years)	62.07 ± 9.30
Sex, male/female	38/19
Type of the poorer performing eye (n)	Right (30), left (27)
MD of the poorer performing eye, mean ± SD (dB)	−15.1 ± 9.5
PSD of the poorer performing eye, mean ± SD (dB)	9.5 ± 4.3
VFI of the poorer performing eye, mean ± SD (%)	55.3 ± 32
RNFL of the poorer performing eye, mean ± SD (μm)	63.7 ± 13.3

See text for abbreviations.

et al., 2015]. Indeed, the retina shares developmental, physiological and anatomical features with the brain [London et al., 2013].

Primary open angle glaucoma (POAG) is the most common type of glaucoma in the Caucasian population. Although exact pathophysiology of POAG is not yet fully clear [Chang and Goldberg, 2012], recent studies of advanced magnetic resonance imaging (MRI) have shown that the POAG-related tissue damage might not be limited to retinal ganglion cells. Indeed, white matter (WM) and gray matter (GM) changes were found throughout the central visual system of patients with POAG [Boucard et al., 2009; Chen et al., 2013; Dai et al., 2012; El-Rafei et al., 2011; Engelhorn et al., 2011, 2012; Garaci et al., 2009; Hernowo et al., 2011; Murai et al., 2013; Wang et al., 2013; Zhang et al., 2012; Zikou et al., 2012], questioning the notion that retinal degeneration is the unique neuropathological substrate of this vision disorder. Moreover, a small pilot MRI study on 13 patients with severe POAG has recently shown microstructural, atrophic and functional brain changes within and outside the visual system [Frezzotti et al., 2014], suggesting that in POAG the neurodegenerative process might be not restricted to the visual system, but also involve other brain systems as it occurs in typical neurodegenerative conditions. In line with this, evidence of a close link between glaucoma and Alzheimer disease, amyotrophic lateral sclerosis and Parkinson disease have been reported in a number of recent experimental studies [Gupta and Yucel, 2007; Jindal, 2013; Ray and Mookherjee, 2009] and the prevalence of glaucoma seems to be much higher in Alzheimer disease patients than in the normal population [Bayer et al., 2002]. We hypothesize that significant and widespread neurodegeneration might occur in glaucoma, spreading across the brain similarly to the typical neurodegenerative conditions [Hardy and Revesz, 2012].

Against this background, we studied here a population of patients covering the different stages of POAG with the aim of assessing: (i) whether tissue damage can really occur within and beyond the visual system, (ii) whether this is only a late event or can be found, perhaps with different degrees, also at early disease stage, and (iii) whether the tissue damage occurring within and beyond the visual system at different disease stages is of any clinical relevance. We, therefore, investigated the presence of brain damage in POAG using multimodal MRI and modeled measures of anatomical connectivity (AC) along WM tracts with those of regional GM volumes and functional connectivity (FC) of resting state networks (RSN). Moreover, we assessed clinical relevance of brain changes by correlating MRI measures with classical opthalmologic measures.

MATERIALS AND METHODS

Study Subjects

We enrolled 86 subjects, of whom 57 POAG patients (Table I) and 29 normal controls (NC, 15 males and 14 females, age = 58 ± 10 years). Patients were recruited among those who were consecutively referring to the Glaucoma Service of the University of Siena and were classified as POAG in presence of typically abnormal optic nerve head, typical glaucomatous visual field loss, open angle at gonioscopy, and no clinically apparent secondary cause of glaucoma. All patients were on pharmacological treatment for glaucoma at study entry. Inclusion criteria for POAG patients were: age between 40 and 80 years, corneal thickness between 520 and 580 μm, glaucomatous damage to the optic nerve and glaucomatous visual field damage. All patients had visual field defects that were reproducible on multiple repeat testing. Exclusion criteria, conversely, were age > 80 years, any ocular disorder other than glaucoma, any neurological disorder (documented clinically and instrumentally), and use of medications that can affect the visual field. POAG patients were classified according to the Hodapp/Bascom Palmer classification [Hodapp et al., 1993].

Subjects in the NC group were recruited among laboratory and hospital workers, had normal neurological and ophthalmological examinations and no history of neurological or ophthalmological disorders.

The study received approval from the local Ethics Committee (Azienda Ospedaliera Universitaria Senese). Informed written consent was obtained from all subjects before study entry.

MRI Acquisition

In all subjects, brain MRI was acquired at the NMR Center of the University of Siena on a 1.5 Tesla Philips Gyroscan (Philips Medical Systems, Best, The Netherlands). A sagittal survey image was used to identify the anterior and posterior commissures. Sequences were acquired in the axial plane parallel to the commissural line. A dual-echo, turbo spin-echo sequence (repetition time [TR]/echo

time [TE]1/TE2 = 2,075/30/90 ms, voxel size = 1 × 1 × 3 mm) yielded proton density and T2-W images. DTI data consisted of echo-planar imaging (EPI) (TR = 8,500 ms; TE = 100 ms; voxel size = 2.5 mm^3), with diffusion weighting distributed in 32 directions and b-value = 1,000 sec mm^{-2}. The resting-fMRI data were 190 volumes of EPI sequence with TR = 1,000 ms, TE = 50 ms, voxel size = 3.75 × 3.75 × 6 mm. A high-resolution T1-weighted image (TR = 25 ms, TE = 4.6 ms, voxel size = 1 mm^3) was acquired for image registration, anatomical mapping and analysis of GM volume.

MRI and Resting fMRI Data Analysis

It was performed with tools of the FMRIB Software Library (FSL, www.fmrib.ox.ac.uk/fsl/) [Jenkinson et al., 2012; Smith et al., 2004].

Microstructure along WM tracts

It was assessed through voxelwise analysis of DTI data using Tract-Based Spatial Statistics (TBSS) [Smith et al., 2006] version 1.2. First, DTI data were corrected for MRI eddy currents and head motion using affine registration to a reference volume, that is, the volume without diffusion weighting ($b = 0$). Second, images of fractional anisotropy (FA), axial diffusivity (AD), and radial diffusivity (RD) were created by fitting a tensor model to the raw DTI data using FDT (FMRIB Diffusion Toolbox) [Behrens et al., 2003] and then brain-extracted using BET (Brain Extraction Tool) [Smith, 2002]. All subjects' FA data were then aligned into a common standard space (FMRIB58_FA) using FNIRT (FMRIB Nonlinear Image Registration Tool) [Andersson et al., 2007a,b]. Next, the mean FA image was created and thinned to create a mean FA skeleton (thresholded at FA > 0.2), which represents the centers of all WM tracts common to the study group, thus avoiding to consider voxels at the edges of the tracts, that may suffer from partial volume effects. Aligned FA data from all study subjects was then projected onto this WM skeleton. TBSS was also applied to the other DTI-derived data (i.e., AD and RD). To achieve this, we used FA images for nonlinear registration, skeletonization and projection stages. The resulting projected (onto the mean WM skeleton) data of all DTI images were finally fed into voxelwise group statistics. See Statistics paragraph for details.

GM volume

Analysis was performed with FSL-VBM [Douaud et al., 2007] version 1.1, which uses an optimized VBM protocol [Good et al., 2001]. First, T1-W images from all study subjects were brain-extracted with BET [Smith, 2002] and GM-segmented [Zhang et al., 2001] before being registered onto the MNI152 standard space using FNIRT [Andersson et al., 2007a,b]. The resulting images were averaged to create a symmetric, study-specific GM template. Second, all native GM images were nonlinearly registered onto this template and "modulated" to correct for local expansion or contraction due to the nonlinear component of the spatial transformation. The modulated GM images were then smoothed with an isotropic Gaussian kernel with a sigma of 3 mm. Because of the use of modulated data, absolute amount (volume) of GM was obtained [Good et al., 2001]. See Statistics paragraph for voxelwise analysis of GM volume.

FC in RSN

Analysis was carried out across the whole brain using probabilistic independent component analysis (PICA) [Beckmann and Smith, 2004] of MELODIC (Multivariate Exploratory Linear Decomposition into Independent Components). Pre-processed data were temporally concatenated across subjects to create a single 4D dataset. Such dataset was variance-normalized and then decomposed into a set of 27 independent components (ICs), where the number of dimensions was automatically estimated using the Laplace approximation to the Bayesian evidence of the model order [Beckmann and Smith, 2004]. ICs of interest were selected by visual inspection and by comparison with previously defined RSNs [Balenzuela et al., 2010; Beckmann et al., 2005; Damoiseaux et al., 2006; De Luca et al., 2006; Rytty et al., 2013]. The remaining ICs represented physiological noise (cardiac, respiratory and cerebrospinal fluid pulsations, head motion), misregistration and scanner-related artifacts and were thus discarded before further processing. Finally, voxelwise analysis of resting-fMRI data was performed using the "dual-regression" approach [Beckmann et al., 2009]. See Statistics paragraph for details.

Visual field measurements

In patients with POAG, at least two reliable standard automated perimetry (SAPs) visual fields were recorded using the Humphrey Field Analyser (Carl Zeiss Meditec, Dublin, CA, USA) running the 30-2 program SITA (Swedish Interactive Threshold Algorithm)-Standard, a standard method for the examination of the 30°central visual field. In this type of measurement, the subject is facing a white illuminated sphere, on which points of light with varying intensities are briefly flashed. Subjects respond when they perceive the flash. The sensitivity at each location in the visual field is determined by changing the intensity of the flash on subsequent presentations. Each eye is measured independently so that one eye is covered while the other is tested. This test provides visual field indices such as: (i) Mean Deviation (MD), which refers to the average deviation of sensitivity at each test location from age-adjusted normal population values, providing an indication of the degree of the generalized loss in the visual field; (ii) Pattern Standard Deviation (PSD), which is a summary measure of the average deviation of individual visual field

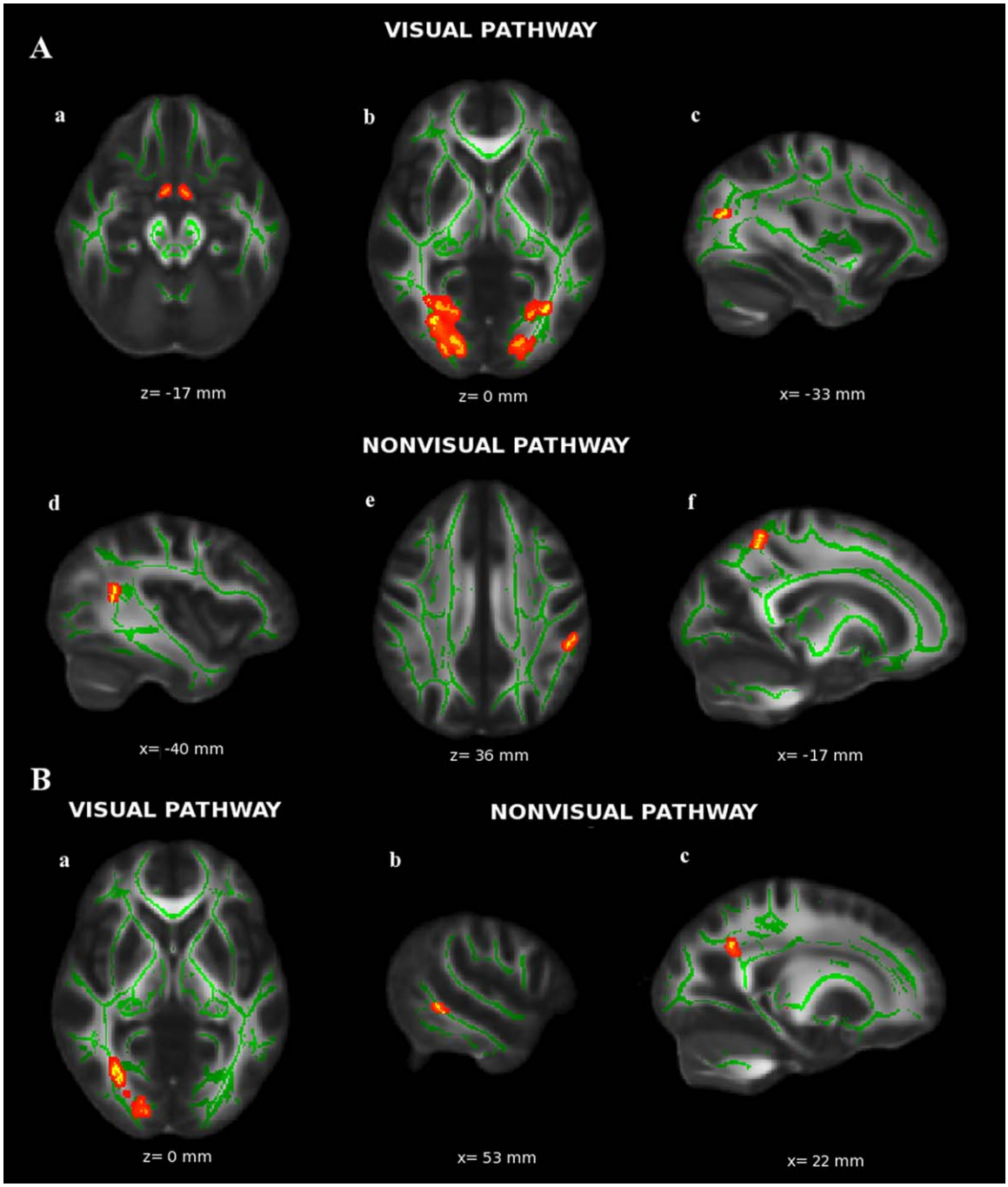

Figure 1.

Tract-Based Spatial Statistics comparison of all-stage (**A**) and early (**B**) POAG patients with NC. Red-yellow shows clusters where both POAG groups have, compared with NC, significant DTI abnormalities (lower FA or higher AD) in the visual pathway (optic tracts [**Aa**], optic radiations [**Ab**, **Ba**], WM of the lateral occipital cortex [**Ac**]) and nonvisual pathway (superior longitudinal fascicle [**Ad**, **Bb**], WM of supramarginal gyrus [**Ae**], superior parietal lobule [**Af**] and precuneous [**Bc**]). Green is the WM skeleton. Background is FMRIB58_FA standard space image (1 mm^3), shown in radiological convention. The most informative slices are shown. See Results and Tables II and III for more details and text for abbreviations. [Color figure can be viewed at wileyonlinelibrary.com]

TABLE II. Regions of the cerebral WM tracts where patients with all-stage POAG showed significant DTI abnormalities with respect to NC at TBSS across the whole brain

	Side	MNI *X*, *Y*, *Z* (mm)	Cluster size (voxel no.)	*P*-value
WM regions of the visual pathways (local maxima)				
Lower FA				
Optic tract	L	−4,7,−22	76	<0.001
	R	4,7,−21	54	<0.001
Optic radiation (inferior fronto-occipital fascicle)	R	16,−81,−4	530	<0.001
	L	−17,−82,−4	130	<0.001
	L	−32,−63,0	72	0.002
Optic radiation (inferior longitudinal fascicle)	L	−11,−86,−4	130	<0.001
	R	28,−77,2	530	<0.001
WM (inferior longitudinal fascicle) of lateral occipital cortex (superior)	L	−33,−71,18	51	<0.001
	L	−24,−64,31	110	<0.001
Higher AD				
Optic tract	L	−2,7,−22	64	<0.001
	R	3,9,−21	50	<0.001
Optic radiation (inferior fronto-occipital fascicle)	R	40,−15,−11	60	0.001
WM regions outside the visual pathways (local maxima)				
Lower FA				
Superior longitudinal fascicle (parietal)	R	39,−52,21	50	0.001
Higher AD				
Superior longitudinal fascicle (temporal)	R	58,−39,−3	67	<0.001
WM of supramarginal gyrus (superior longitudinal fascicle)	L	−48,−39,40	50	0.001
WM of superior parietal lobule (superior longitudinal fascicle)	L	−16,−50,60	65	0.001

For each DTI measure, WM regions are ordered according to increasing *Z* values. See text for details (including values of DTI measures) and abbreviations.

sensitivity values from the normal slope after correcting for any overall sensitivity differences; and (iii) Visual Field Index (VFI), a new global metric representing the entire visual field as a percentage of normal. Abnormal SAP results were defined as typical glaucomatous defects with a PSD significantly increased beyond the 5% level and/or a Glaucoma Hemifield Test result outside normal limits.

Optical coherence tomography. Peripapillary RNFL thickness was measured using the Optic Disc Cube 200 × 200 scanning protocol of the Cirrus OCT (Carl Zeiss Meditec, Dublin, CA). For image acquisition, scanning laser images were focused after subjects were seated and properly positioned. OCT is based on light, which unlike sound waves used in B-mode ultrasonography does not require contact with the tissue to be examined. It measures the delay in the echo and the intensity of diffused light, that is, the light reflected by tissue microstructure, using a wavelength of about 820 nm. The image is captured in a few seconds and requires steady fixation by the patient. The structures visualized are the result of selective absorption and selective reflection by the structure or the interface illuminated by the laser. This can depend on the type of structures (the most reflective are the RNFL, and on the direction of the incident ray (when structures are perpendicular to the ray, reflectivity is greater, indicated in red in OCT images).

Statistics

As for general statistics, differences in age, head movement parameters during resting-fMRI acquisition between POAG patients and NCs were tested with Mann–Whitney test. Fisher's test was used for between-group comparisons of sex, grade of WM hyperintensities, presence/absence of hypertension. Data were considered significant at $P < 0.05$. SPSS was used to perform such statistical analyses.

As for voxelwise analyses of DTI measures, GM volume and RSN-FC, comparisons of POAG patients with NCs and correlations with disease stage and ophthalmological measures (visual field and RNFL) in the poorer performing eye of all patients were carried out in the general linear model framework with, respectively, unpaired *t*-tests and regression analyses using FSL randomize, a nonparametric permutation testing (5,000 permutations). The level of significance for all analyses was set at $P < 0.005$, uncorrected, cluster size ≥ 50 voxels using threshold-free cluster enhancement. Subsequently, to further confirm our results we computed within significant clusters of between-group comparisons mean values across all voxels in each subject

TABLE III. Regions of the cerebral WM tracts where patients with early stage (Stage 1) POAG showed significant DTI abnormalities with respect to NC at TBSS across the whole brain

	Side	MNI X, Y, Z (mm)	Cluster size (voxel no.)	P-value
WM regions of the visual pathways (local maxima)				
Lower FA				
Optic radiation (inferior fronto-occipital fascicle)	L	−35,−35,5	166	<0.001
Higher AD				
Optic radiation (inferior fronto-occipital fascicle)	R	36,−51,−3	52	0.002
	R	31,−62,0	58	<0.001
WM of the occipital pole (forceps major)	R	21,−86,2	89	<0.001
WM regions outside the visual pathways (local maxima)				
Higher AD				
Superior longitudinal fascicle (temporal)	R	53,−41,−5	97	<0.001
WM of precuneous	R	23,−57,31	72	<0.001

For each DTI measure, WM regions are ordered according to increasing Z values. See text for details (including values of DTI measures) and abbreviations.

and applied analysis of variance, using Bonferroni correction for multiple comparisons. Moreover, nonparametric Spearman correlation was used to quantify in all patients with POAG the strength of correlation in clusters of brain abnormalities with measures of disease stage and ophthalmologic measures in the poorer performing eyes.

In all analyses, age, sex, grade of WM hyperintensities, presence/absence of hypertension were used as covariates.

WM and GM regions corresponding to local maxima within significant clusters were anatomically mapped using standard-space atlases provided by FSL (JHU DTI-based WM atlases for WM; Harvard-Oxford cortical/subcortical structural atlases for GM).

RESULTS

General

All patients had bilateral POAG and clinical characteristics of the poorer performing eyes as well as demographics are reported in Table I. According to the Hodapp/Bascom Palmer classification, POAG patients had early (Stage 1, $n = 14$), moderate (Stage 2, $n = 13$), and severe (Stage 3, $n = 30$) disease.

No significant differences were found between POAG patients and NC in terms of age ($P = 0.1$), sex ($P = 0.24$), occurrence of hypertension (30% vs. 25%, $P = 0.61$), and MRI WM hyperintensities, assessed with Fazekas scale [Fazekas et al., 1987] (grade 0: 70% vs. 73%, $P = 0.9$; grade 1: 25% vs. 24%, $P = 0.9$; grade 2: 5% vs. 3%, $P = 0.9$; no grade 3 in either groups).

Comparisons between POAG Patients and NCs

Microstructure along WM tracts

At TBSS analysis across the whole brain (Fig. 1A and Table II), POAG patients showed lower FA than NC along the visual pathway (0.35 ± 0.02 vs. 0.40 ± 0.02, $P < 0.001$), namely in the optic tracts (OT), optic radiations (OR) mapping on the inferior fronto-occipital fascicle (IFOF), and inferior longitudinal fascicle (ILF), and in the WM adjacent to the lateral occipital cortex, containing fibers from ILF. POAG patients also showed higher AD than NCs along the visual pathway in the OT and OR (IFOF) (1.85 ± 0.15 vs. 1.68 ± 0.12 mm^2/sec, $P < 0.001$).

TBSS analysis showed DTI abnormalities in POAG patients also beyond the visual pathway. In particular, there was lower FA (0.46 ± 0.04 vs. 0.52 ± 0.03, $P < 0.001$) in the superior longitudinal fascicle (SLF, parietal part) and higher AD (1.05 ± 0.05 vs. 0.95 ± 0.05 mm^2/sec, $P < 0.001$) in the SLF (temporal part), WM of supramarginal gyrus and superior parietal lobule, containing fibers from SLF.

To investigate whether microstructural abnormalities along WM tracts were present early in the disease, a subgroup analysis of patients with stage-1 POAG was performed. Results showed lower FA and higher AD in this patient subgroup than in NC across the brain. Similarly to the whole POAG population, abnormalities mapped along the visual pathway (FA: 0.45 ± 0.02 vs. 0.49 ± 0.02, $P < 0.001$; AD: 1.30 ± 0.04 vs. 1.21 ± 0.03 mm^2/sec, $P < 0.001$) and beyond the visual pathway (AD: 1.10 ± 0.01 vs. 1 ± 0.006 mm^2/sec, $P < 0.001$) (see Fig. 1B and Table III for details)

GM Volume

No difference in GM volume was found between the whole group of POAG patients and NC. However, when the analysis was restricted to the subgroup of patients with severe disease (stage-3 POAG), results showed lower GM volume in visual-related regions (occipital fusiform gyrus and lateral occipital cortex [LOC, superior]; 508 ± 90 mm^3 vs. 603 ± 75 mm^3, $P < 0.001$) and in the

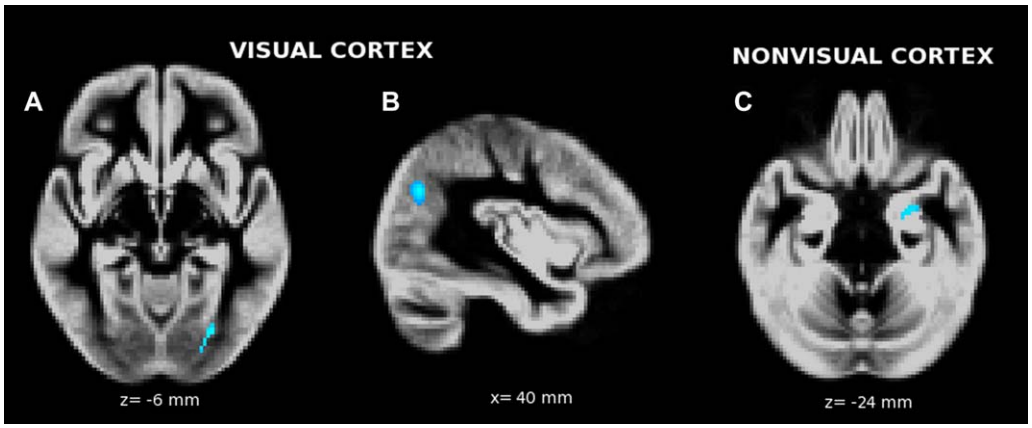

Figure 2.

FSL-Voxel Based Morphometry comparison of severe POAG patients with NC. Blu-light blu shows clusters where patients with stage-3 POAG have, compared with NC, significantly lower GM volume in the visual cortex (occipital fusiform gyrus [**A**] and lateral occipital cortex [**B**]) and nonvisual cortex (hippocampus [**C**]). Background is the study-specific template in standard space (2 mm^3), shown in radiological convention. The most informative slices are shown. See Results and Table IV for more details and text for abbreviations. [Color figure can be viewed at wileyonlinelibrary.com]

hippocampus (337 ± 37 mm^3 vs. 391 ± 42 mm^3, $P < 0.001$) (Fig. 2 and Table IV).

FC in RSN

No difference was found between POAG patients and NCs in the head movement parameters during resting-fMRI acquisition (relative displacement: 0.08 ± 0.05 mm vs. 0.08 ± 0.07 mm, $P = 0.68$; absolute displacement: 0.28 ± 0.13 mm vs. 0.30 ± 0.23 mm, $P = 0.18$). PICA across the whole brain of the study population defined 13 functionally relevant RSNs, including visual network (VN), auditory network, sensorimotor network, default mode network (DMN, anterior and posterior), working memory network (WMN, right and left), fronto-medial and orbitofrontal networks, executive control network, salience network, subcortical network (ScN), temporal pole network. Four of these RSNs showed significant between-group differences in terms of FC (Fig. 3A and Table V). In particular, POAG patients had lower FC in the VN (17.16 ± 10.41 vs. 25.9 ± 14.8, $P = 0.002$) and in the WMN (7.48 ± 5.35 vs. 13.45 ± 6.34, $P < 0.001$). Conversely, POAG patients had higher FC than NC in the DMN (12.67 ± 8.76 vs. 5.93 ± 10.74, $P = 0.002$) and in the ScN (15.13 ± 7.23 vs. 8.68 ± 6.74, $P < 0.001$).

Similarly to AC, abnormalities in FC were already present in the subgroup of patients with stage-1 POAG. In particular, lower levels were found in various RSNs, including VN (29.8 ± 10.47 vs. 45.63 ± 31.91, $P = 0.01$), WMN (5.77 ± 3.56 vs. 11.62 ± 6.63, $P = 0.004$ on the right, 8.77 ± 1.32 vs. 14.82 ± 0.92, $P = 0.001$ on the left) and DMN (5.73 ± 4.91 vs. 13.78 ± 8.05, $P = 0.001$), whereas a higher level was present in the ScN (13.79 ± 7.98 vs. 8.12 ± 6.40, $P = 0.016$) (see Fig. 3B and Table VI for details).

TABLE IV. Regions of the cerebral GM where patients with severe (Stage 3) POAG showed significant decrease in volume (i.e., atrophy) with respect to NC at FSL-VBM across the whole brain

	Side	MNI *X*, *Y*, *Z* (mm)	Cluster size (voxel no.)	*P*-value
GM regions of the visual cortex (local maxima)				
Occipital fusiform gyrus	L	−28,−76,−4	50	0.003
Lateral occipital cortex (superior)	R	36,−64,24	210	0.002
	R	52,−68,38	191	0.001
GM regions outside the visual cortex (local maxima)				
Hippocampus	L	−26,−10,−20	72	0.005

GM regions of each set are ordered according to increasing *Z* values. See text for details (including values of GM volumes) and abbreviations.

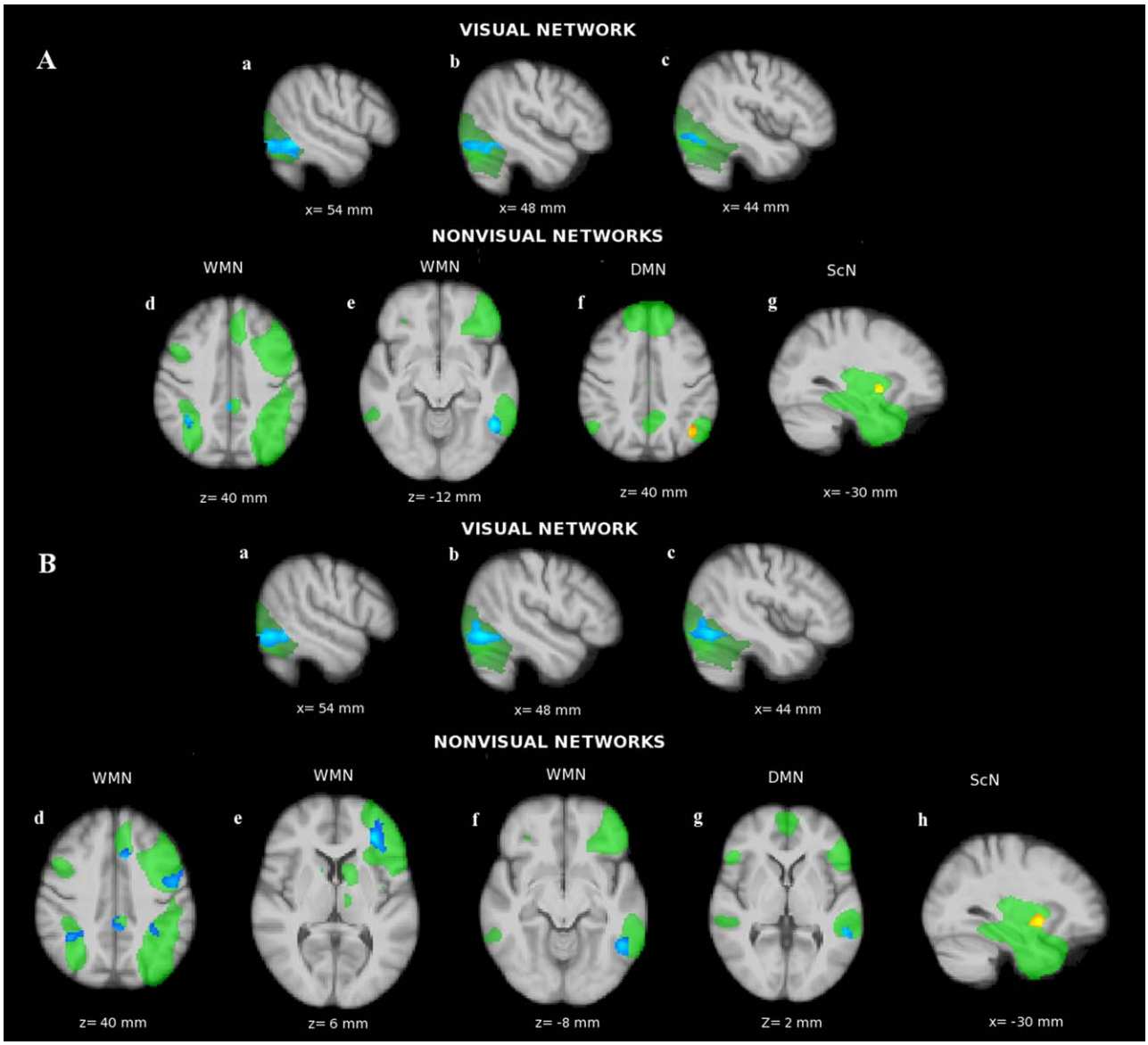

Figure 3.

Resting state network functional connectivity comparison of all-stage (**A**) and early (**B**) POAG patients with NC. Blu-light blu and red-yellow show clusters where POAG patients have, respectively, significantly lower and higher functional connectivity than NC in different brain networks (in green), including visual network (VN, **Aa**–**Ac**, **Ba**–**Bc**) and nonvisual networks (working memory network [WMN, **Ad-Ae**, **Bd**–**Bf**], default mode network [DMN, **Af**, **Bg**] and subcortical network [ScN, **Ag**, **Bh**]). Background image, shown in radiological convention, is the average of high-resolution structural images transformed into standard space (MNI152, 2 mm^3). The most informative slices are shown. See Results and Tables V and VI for more details and text for abbreviations. [Color figure can be viewed at wileyonlinelibrary.com]

Correlations of Brain Abnormalities with Glaucoma Stage

Voxelwise correlations were found between some of the structural abnormalities across brain and increasing POAG stage (Fig. 4 and Table VII).

As for the visual system, there was a worsening in WM microstructure (lower FA and higher AD) along OR (IFOF) ($r = -0.55$, $P < 0.001$ for FA; $r = 0.43$, $P < 0.001$ for AD). Outside the visual system, increasing POAG stage correlated with higher AD in the SLF ($r = 0.56$, $P < 0.001$) and

TABLE V. GM regions of the RSNs where patients with all-stage POAG showed significant abnormalities in functional connectivity with respect to NC at probabilistic ICA across the whole brain

	Side	MNI *X*, *Y*, *Z* (mm)	Cluster size (voxel no.)	*P*-value
GM regions of the visual network (local maxima)				
Lower FC				
Visual network				
Fusiform cortex (temporo-occipital)	R	34,−34,−24	81	0.001
Inferior temporal gyrus (temporo-occipital)	R	56,−52,−24	756	<0.001
Lateral occipital cortex (inferior)	R	50,−80,4	88	<0.001
GM regions outside the visual network (local maxima)				
Lower FC				
Working memory network				
Posterior cingulate cortex	R	2,−38,−36	74	0.001
Inferior temporal gyrus	L	−46,−56,−12	94	0.001
Angular gyrus	R	38,−52,40	57	0.002
Higher FC				
Default mode network				
Lateral occipital cortex (superior)	L	−34,−64,40	93	0.001
Subcortical network				
Putamen	L	−30,4,0	50	0.003

Clusters in each RSN are ordered according to increasing *Z* values. See text for details (including values of functional connectivity) and abbreviations.

lower GM volume in the hippocampus and various frontal regions ($r = -0.58$, $P < 0.001$)

Correlation of Brain Abnormalities with Ophthalmologic Measures

Lower RNFL values showed voxelwise correlations with abnormalities in the visual system (Fig. 5 and Table VIII): lower FA in the OR (ILF) ($r = 0.40$, $P = 0.003$) and lower GM volume in the LOC (inferior) ($r = 0.32$, $P = 0.02$). In addition, lower RNFL values showed voxelwise correlation with abnormalities outside the visual system (Fig. 5 and Table VIII): lower FA in the splenium of the corpus callosum and WM of the postcentral gyrus ($r = 0.50$, $P < 0.001$) and lower GM volume in the cerebellum, temporal fusiform gyrus, inferior temporal gyrus, caudate, postcentral gyrus and frontal pole ($r = 0.32$, $P = 0.02$).

Regarding visual field, higher PSD showed correlation (Fig. 5 and Table VIII) with lower FC in the VN (LOC and superior temporal gyrus) ($r = -0.33$, $P = 0.01$).

DISCUSSION

In this multimodal MRI study, we provided evidence of widespread structural and functional brain changes in a group of POAG patients covering all disease stages. Interestingly, changes in some brain areas showed a relationship with ophthalmologic measures and a worsening through the disease stages. Of paramount importance, both structural and functional abnormalities of brain connectivity were present also in the early POAG stage.

Changes in the Visual System

Microstructure along WM tracts

The whole visual pathway of our POAG population showed AC microstructural abnormalities, in line with both human [Chen et al., 2013; El-Rafei et al., 2011; Engelhorn et al., 2011, 2012; Garaci et al., 2009; Murai et al., 2013; Zikou et al., 2012] and experimental [Crish and Calkins, 2015] studies and most of these changes already occurred at early stage. Reduction of FA, a measure of WM tract integrity, and/or increase of AD, a putative marker of axonal damage/loss were found in the OT, OR (IFOF/ILF), and occipital WM containing OR fibers. OT carry retinal information on the whole visual field whereas IFOF and ILF play roles in visuospatial function and memory. A further evidence of damage to the visual pathway of POAG comes from a proton MR spectroscopy study which not only demonstrated in the geniculocalcarine WM but also in the striate GM of occipital lobe a significant decrease in *N*-acetylaspartate and choline, consistent with axonal damage/loss and reduced cell density, respectively [Zhang et al., 2013]. The damage along OR since the early POAG stage is in agreement with experimental models of disease, where one of the earliest pathogenic events, even before axonal degeneration in the optic nerve and RGC body loss, is decreased active axonal transport from retina to the brain [Crish et al., 2010; Ward et al., 2014].

GM volumes

No atrophy was found in the visual cortex of POAG. However, this was shown in the severe stage, in line with

TABLE VI. GM regions of the RSNs where patients with early-stage (Stage 1) POAG showed significant abnormalities in functional connectivity with respect to NC at probabilistic ICA across the whole brain

	Side	MNI *X*, *Y*, *Z* (mm)	Cluster size (voxel no.)	*P*-value
GM regions of the visual network (local maxima)				
Lower FC				
Visual network				
Inferior temporal gyrus	R	60,−56,−22	1435	<0.001
Lateral occipital cortex (inferior)	R	48,−72,−16		<0.001
GM regions outside the visual network (local maxima)				
Lower FC				
Working memory network				
Inferior temporal gyrus	L	−50,−58,−12	124	<0.001
Frontal pole	L	−36,40,6	1030	<0.001
	R	20,50,30	87	0.001
Posterior cingulate	R	2,−34,34	154	<0.001
Paracingulate gyrus	L	−8,20,38	156	<0.001
Superior parietal lobule	R	30,−46,40	57	<0.001
	L	−34,−46,46	367	<0.001
Precentral gyrus	L	−48,4,48	804	<0.001
Precuneous	L	−4,−76,48	91	<0.001
Default mode network				
Middle temporal gyrus	R	58,−18,−10	53	0.001
	L	−60,−44,4	167	0.002
Higher FC				
Subcortical network				
Putamen	L	−26,8,−4	267	<0.001

Clusters in each RSN are ordered according to increasing *Z* values. See text for details (including values of functional connectivity) and abbreviations.

previous studies [Bogorodzki et al., 2014; Boucard et al., 2009; Frezzotti et al., 2014; Li et al., 2012; Zikou et al., 2012] and mapped on postero-lateral regions such as the occipital fusiform gyrus and LOC, both involved in cognition (color information processing, face/body and object recognition) [Grill-Spector et al., 2001]. Interestingly, occipital fusiform gyrus lies close to OR, which indeed showed DTI abnormalities and this would support the occurrence of a secondary anterograde transynaptic degeneration primed by RGCs loss, as demonstrated in experimental animal models [Lam et al., 2003] and postmortem studies [Gupta et al., 2006]. However, a primary neurodegenerative process of the visual cortex followed by retrograde transynaptic degeneration cannot be entirely ruled out.

FC at network level

Our POAG group showed decreased FC in the VN, which similarly to AC microstructural changes along visual pathway, also occurred at early stage. This finding might be secondary to reduced visual information and/or to transynaptic degeneration of connected WM tracts and is consistent with recent studies using different approaches of resting-fMRI such as FC analysis from regions of interest [Dai et al., 2012], amplitude of low frequency fluctuations [Li et al., 2014], regional homogeneity [Song et al., 2014], and temporal dynamics of brain synchronization [Bola et al., 2015].

Correlation with disease stages and ophthalmologic measures

In our POAG group worsening DTI measures along OR correlated with evolving disease stage, suggesting a progressive accrual of the microstructural damage in the posterior visual pathway. These findings are in general agreement with previous studies [Dai et al., 2013; Michelson et al., 2013] and demonstrate the potential usefulness of DTI as a noninvasive tool for tracking POAG severity.

In terms of clinical relevance, retinal thinning correlated with lower FA along OR and LOC atrophy. This is not surprising, as these structures are anatomically connected and it would confirm the presence of a "neurodegenerative path" linking these brain regions to the eye, with a mechanism of anterograde and/or retrograde transynaptic degeneration.

Finally, altered visual field (increased PSD) correlated with lower FC in the VN (LOC), reflecting a reduced cortical integration of visual information and/or a possible exhaustion of functional cortical reorganization.

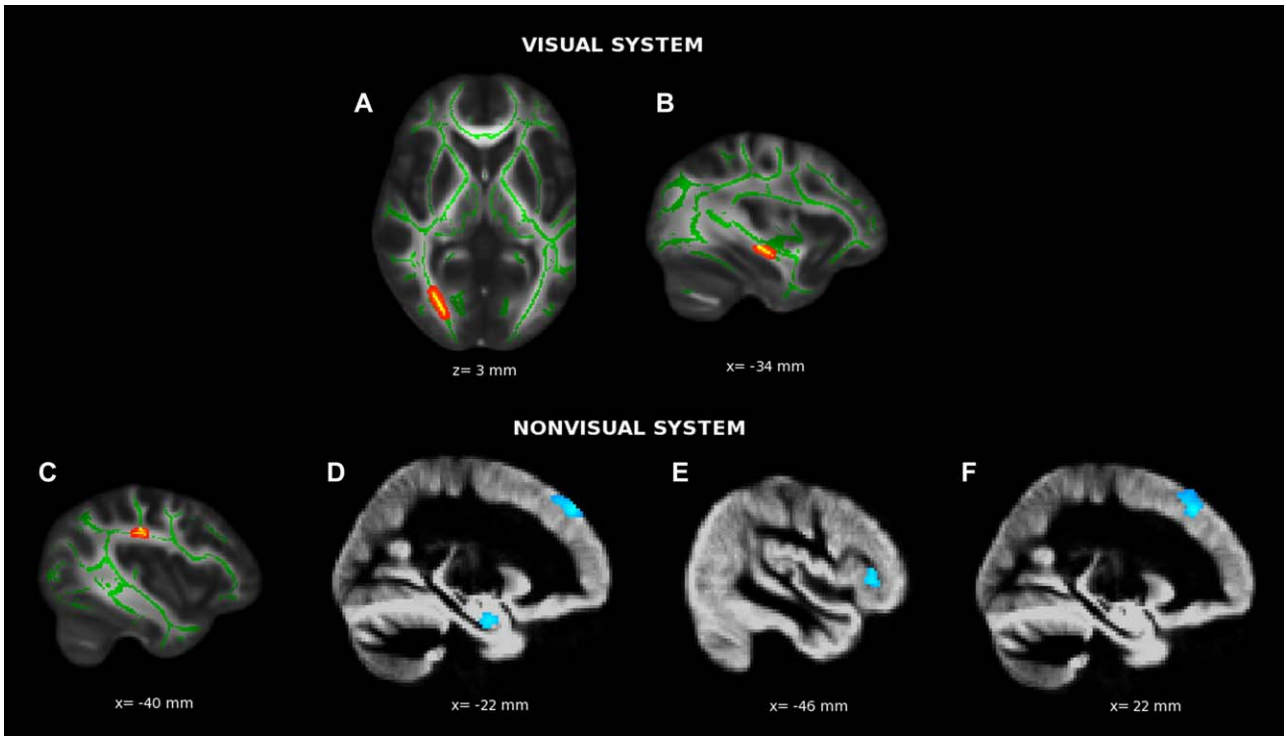

Figure 4.

Clusters showing significant correlations between increasing POAG stage and MRI abnormalities in the visual system (lower FA [**A**] and higher AD [**B**] in the optic radiation) and nonvisual system (higher AD in the superior longitudinal fascicle [**C**], lower GM volume in the hippocampus and various regions of the frontal cortex [**D**–**F**]). Background images for the different MRI modalities are in standard space (1 mm^3 for TBSS, 2 mm^3 for FSLVBM) and radiological convention. The most informative slices are shown. See Results and Table VII for more details and text for abbreviations. [Color figure can be viewed at wileyonlinelibrary.com]

Changes Outside the Visual System

Microstructure along WM tracts

Microstructural AC changes were found in the whole POAG group and at early stage along WM tracts that are not part of the typical visual pathway but somehow related with visual processing (parietal SLF and precuneous WM). SLF provides the prefrontal cortex with information on visual space and supplies the parietal cortex (superior parietal lobule, precuneous) with information on spatial location of body parts to regulate higher motor behavior.

Interestingly, however, our POAG group also showed since the early stage unanticipated anomalies along WM tracts unrelated to vision and involved in episodic memory retrieval (precuneous) and language processing (temporal SLF, supramarginal gyrus WM).

GM volumes

We observed hippocampal atrophy only in the severe POAG, in line with our recent MRI pilot study [Frezzotti et al., 2014]. Hippocampus plays important roles for memory and spatial orientation. Indeed, it is connected to regions of the visual cortex such as fusiform gyrus, where atrophy occurred in our POAG group, by ILF fibers [Catani et al., 2003], which also showed here altered DTI measures. Importantly, hippocampus is one of the earliest regions in the Alzheimer brain to show neurodegeneration, including deposition of intracellular tau proteins (neurofibrillary tangles) and extracellular amyloid-β and subsequent transynaptic spreading toward distant brain regions [Hardy and Revesz, 2012].

FC at network level

Outside the typical VN, we found in our POAG group decreased FC in a RSN mainly subserving working memory but also involved in top-down executive control [Vincent et al., 2008] and in visual processing. Indeed, such RSN mainly comprises fronto-parietal regions of the "dorsal visual stream," engaged in spatial information and motion orientation. Interestingly, impaired resting state in the posterior cingulate cortex was found closely associated with Alzheimer disease progression [Liu et al., 2014; Wang

TABLE VII. Brain regions showing correlation between changes in anatomical connectivity, GM volume, and increasing stage of POAG

	Side	MNI *X*, *Y*, *Z* (mm)	Cluster size (voxel no.)	*P*-value
Regions of the visual system (local maxima)				
Lower FA				
Optic radiation (inferior fronto-occipital fascicle)	R	31,−69,0	158	<0.001
Higher AD				
Optic radiation (inferior fronto-occipital fascicle)	L	−34,−20,−8	68	*<0.001*
Regions outside the visual system (local maxima)				
Higher AD				
Superior longitudinal fascicle	L	−42,−21,30	88	0.001
Lower GM volume				
Hippocampus	L	−18,−6,−24	135	0.002
Inferior frontal gyrus	L	−46,30,0	55	0.003
Frontal pole	L	−12,40,40	582	<0.001
Superior frontal gyrus	R	22,30,60	97	0.002

For each MRI measure, brain regions are ordered according to increasing *Z* values. See text for details (including *r* values) and abbreviations.

et al., 2011]. In general, this complex RSN is part of the so-called "external attention system" (EAS), which mediates attention to exogenous stimuli and effortful encoding of short-term information in contrast with DMN, which supports internally-oriented processes, including constant and "off-line" memory consolidation [Golland et al., 2008]. In terms of RSN dynamics, EAS and DMN seem to be functionally anticorrelated and this may explain in our

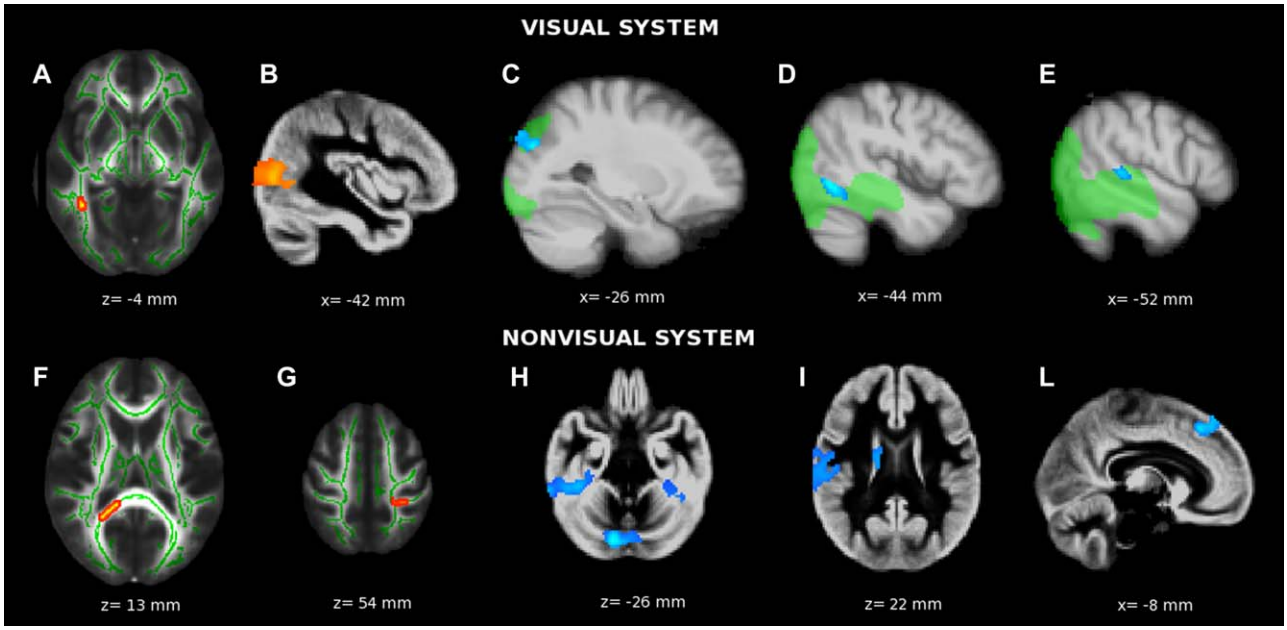

Figure 5.

Clusters showing in the whole POAG group significant correlations between ophthalmologic measures (RNFL, visual field PSD) and MRI abnormalities in the visual system (lower FA in the optic radiation [**A**]; lower GM volume in the lateral occipital cortex [**B**]; lower FC in the visual network [**C**–**E**]) and nonvisual system (lower FA in the splenium of the corpus callosum [**F**] and WM of the postcentral gyrus [**G**]; lower GM volume in the cerebellum, temporal gyrus, caudate, postcentral gyrus and frontal pole [**H**–**L**]). Background images for the different MRI modalities are in standard space (1 mm^3 for TBSS, 2 mm^3 for FSLVBM and RSN analysis) and radiological convention. The most informative slices are shown. See Results and Table VIII for more details and text for abbreviations. [Color figure can be viewed at wileyonlinelibrary.com]

TABLE VIII. Brain regions where our patients with POAG showed correlations with ophthalmologic measures in poorer performing eyes

	Side	MNI *X*, *Y*, *Z* (mm)	Cluster size (voxel no.)	*P*-value
Regions of the visual system (local maxima)				
Lower RNFL and lower FA				
Optic radiation (Inferior longitudinal fascicle)	R	40,−47,−5	63	0.001
Lower RNFL and lower GM volume				
Lateral occipital cortex (inferior)	L	−32,−84,−2	942	<0.001
Higher PSD and lower FC				
Visual network				
Lateral occipital cortex (inferior)	L	−44,−64,−6	110	<0.001
Superior temporal gyrus	L	−50,−36,6	198	<0.001
Lateral occipital cortex (superior)	L	−26,−82,28	203	<0.001
Regions outside the visual system (local maxima)				
Lower RNFL and lower FA				
Splenium of the corpus callosum	R	16,−42,12	215	<0.001
WM of the postcentral gyrus	L	−23,−35,56	53	<0.001
Lower RNFL and lower GM volume				
Cerebellum	R	16,−76,−30	1825	<0.001
Temporal fusiform gyrus	L	−32,−34,−28	190	0.001
Inferior temporal gyrus	R	48,−34,−20	544	<0.001
Caudate	R	14,−6,18	941	0.001
Postcentral gyrus	R	64,−16,18	1984	<0.001
Frontal pole	L	−12,42,54	144	0.001

Each correlation is ordered according to increasing *Z* values. See text for details (including *r* values) and abbreviations.

POAG group the concurrent and opposite FC anomalies. Indeed, we observed since the early stage in various EAS parts a reduced FC which turned out to be less extensive in the whole patient group whereas FC in the DMN was lower at early stage but increased in the whole group, all changes that might represent a failed attempt of compensatory functional reorganization and thus a possible "maladaptation" toward the POAG clinical worsening. A similar reason could explain, in the whole POAG group, the increased FC within the ScN mapping on the putamen, which alongside motor regulation exerts a role in various types of learning [Packard and Knowlton, 2002]. Conversely, the increased FC in the same RSN in the early POAG group can be viewed as an attempt of adaptive functional reorganization at an early stage of brain pathology.

Correlation with disease stages and ophthalmologic measures

In terms of AC, increasing AD was found through disease stages along the SLF whereas progressive GM volume reduction was shown in the hippocampus. These findings point toward a progressive neurodegeneration in unanticipated brain structures and thus a widespread pathology in the POAG brain. In addition, the voxelwise relationships of retinal damage (RNFL) with AC changes along WM tracts and with atrophy in GM regions far from the visual cortex may be secondary to transynaptic degeneration and pathology spreading.

FC anomalies in nonvisual RSNs, although present, were not directly associated here with ophthalmologic measures and thus, their relevance toward other clinical features (e.g., cognition) of POAG need to be further explored.

Linking POAG with neurodegenerative diseases

The occurrence of widespread and progressive brain abnormalities since the early stage propose POAG as a complex condition, involving unanticipated structures and functions. Importantly, we showed progressive hippocampal volume decrease through the POAG stages, until reaching an atrophic condition in the severe stage. Hippocampus represents the initial site of misfolded proteins accumulation in Alzheimer disease, with subsequent spreading and templating. It is conceivable that such mechanisms, hypothesized for typical neurodegenerative conditions [Hardy and Revesz, 2012], might also occur in the POAG brain and indeed abnormal accumulation of misfolded protein aggregates was reported in the visual system of (both experimental and human) glaucoma and Alzheimer disease [Gupta and Yucel, 2007; Jindal, 2013]. An intriguing but somehow questionable neurodegenerative hypothesis tested recently in animal and cell culture models of Alzheimer disease is that amyloid-β may, on the one hand, play a protective role in innate immunity and, on the other hand, abnormally accumulate in presence of an inflammatory stimulus [Kumar et al., 2016].

Other features shared by POAG and AD are the molecular mechanisms of oxidative/metabolic stress, the loss of specific neuronal populations, glial reactivity [Ghiso et al., 2013], a high rate of POAG occurrence in Alzheimer patients [Bayer et al., 2002] and, more recently, a dysfunction of the "glymphatic" system, a brain-wide paravascular pathway that facilitates clearance of solutes, including amyloid-β, from the brain [Wostyn, et al., 2015].

Study Strengths and Limitations

We selected POAG patients without other ophthalmological/neurological diseases to allow an appropriate assessment of the neurodegeneration spreading. The role of possible confounders was controlled for by matching the study groups and also using them as covariates in the statistical models. Moreover, we applied a robust and sensitive voxelwise approach for the analysis of the different MRI modalities.

A potential limitation is the uncorrected voxelwise thresholding. Indeed, analyses were performed with an "explorative" uncorrected threshold of $P < 0.005$ as no results survived at multiple comparisons correction. However, to reduce false positives, we first selected clusters ≥ 50 voxels, similarly to other studies [Adams et al., 2011; Connally et al., 2013; Frezzotti et al., 2014; Lindner et al., 2014; Loitfelder et al., 2012; Martinez et al., 2013; Wicker et al., 2003] and then, following a previous approach [Anjari et al., 2007; Frezzotti et al., 2014] a full Bonferroni correction was used. A higher number of study subjects, planned for a future study, and longer scan times, especially for resting fMRI, would arguably increase the sensitivity and the effect size of these findings.

CONCLUSION

Our findings demonstrate connectivity changes since early POAG in both visual and nonvisual systems, whereas atrophy is confined to the severe stage. Changes in some of the brain regions correlated with visual severity measures and worsened through disease stages, thus stressing their clinical relevance and calling for different and more complex strategies for the management of POAG patients.

ACKNOWLEDGMENTS

The authors thank Riccardo Tappa Brocci (University of Siena) for help with MRI data acquisition. Conflicts of interest: PF, AG, ADL and FT report no conflicts. NDS has received honoraria for consulting services, speaking, and travel support from Schering, Biogen Idec, Teva, Novartis Pharma AG, Genzyme, and Merck Serono S.A. He serves on ad- visory boards for Merck Serono S.A. and Novartis Pharma AG, and has received research grant support from the Italian MS Society (AISM), Merck Serono S.A., and Novartis Pharma AG

REFERENCES

Adams RB Jr, Franklin RG Jr, Kveraga K, Ambady N, Kleck RE, Whalen PJ, Hadjikhani N, Nelson AJ (2011): Amygdala responses to averted vs direct gaze fear vary as a function of presentation speed. Soc Cogn Affect Neurosci 7:568–577.

Andersson JLR, Jenkinson M, Smith S (2007a): Non-linear optimisation. FMRIB technical report TR07JA1. Available at: www.fmrib.ox.ac.uk/analysis/techrep

Andersson JLR, Jenkinson M, Smith S (2007b): Non-linear registration, aka Spatial normalisation. FMRIB technical report TR07JA2. Available at: www.fmrib.ox.ac.uk/analysis/techrep

Anjari M, Srinivasan L, Allsop JM, Hajnal JV, Rutherford MA, Edwards AD, Counsell SJ (2007): Diffusion tensor imaging with tract-based spatial statistics reveals local white matter abnormalities in preterm infants. Neuroimage 35:1021–1027.

Balenzuela P, Chernomoretz A, Fraiman D, Cifre I, Sitges C, Montoya P, Chialvo DR (2010): Modular organization of brain resting state networks in chronic back pain patients. Front Neuroinform 4:116.

Bayer AU, Ferrari F, Erb C (2002): High occurrence rate of glaucoma among patients with Alzheimer's disease. Eur Neurol 47: 165–168.

Beckmann CF, Smith SM (2004): Probabilistic independent component analysis for functional magnetic resonance imaging. IEEE Trans Med Imaging 23:137–152.

Beckmann CF, DeLuca M, Devlin JT, Smith SM (2005): Investigations into resting-state connectivity using independent component analysis. Philos Trans R Soc Lond B Biol Sci 360:1001–1013.

Beckmann CF, Mackay CE, Filippini N, Smith SM. (2009): Group Comparison of Resting-State FMRI Data Using Multi-Subject ICA and Dual Regression. Organization for Human Brain Mapping Annual Meeting. Neuroimage 47 (supplement 1).

Behrens TE, Woolrich MW, Jenkinson M, Johansen-Berg H, Nunes RG, Clare S, Matthews PM, Brady JM, Smith SM (2003): Characterization and propagation of uncertainty in diffusion-weighted MR imaging. Magn Reson Med 50:1077–1088.

Bogorodzki P, Piatkowska-Janko E, Szaflik J, Szaflik JP, Gacek M, Grieb P (2014): Mapping cortical thickness of the patients with unilateral end-stage open angle glaucoma on planar cerebral cortex maps. PLoS One 9:e93682.

Bola M, Gall C, Sabel BA (2015): Disturbed temporal dynamics of brain synchronization in vision loss. Cortex 67:134–146.

Boucard CC, Hernowo AT, Maguire RP, Jansonius NM, Roerdink JB, Hooymans JM, Cornelissen FW (2009): Changes in cortical grey matter density associated with long-standing retinal visual field defects. Brain 132:1898–1906.

Bussel II, Wollstein G, Schuman JS (2014): OCT for glaucoma diagnosis, screening and detection of glaucoma progression. Br J Ophthalmol 98(Suppl 2):ii15–ii19.

Calabresi PA, Balcer LJ, Frohman EM (2015): Optical Coherence Tomography in Neurologic Diseases. Cambridge University Press, Cambridge, United Kingdom, ISBN 978-1-107-04130-1.

Catani M, Jones DK, Donato R, Ffytche DH (2003): Occipito-temporal connections in the human brain. Brain 126:2093–2107.

Chang EE, Goldberg JL (2012): Glaucoma 2.0: Neuroprotection, neuroregeneration, neuroenhancement. Ophthalmology 119: 979–986.

Chen Z, Lin F, Wang J, Li Z, Dai H, Mu K, Ge J, Zhang H (2013): Diffusion tensor magnetic resonance imaging reveals visual pathway damage that correlates with clinical severity in glaucoma. Clin Exp Ophthalmol 41:43–49.

Connally EL, Ward D, Howell P, Watkins KE (2013): Disrupted white matter in language and motor tracts in developmental stuttering. Brain Lang 131:25–35.

Crish SD, Sappington RM, Inman DM, Horner PJ, Calkins DJ (2010): Distal axonopathy with structural persistence in glaucomatous neurodegeneration. Proc Natl Acad Sci USA 107: 5196–5201.

Crish SD, Calkins DJ (2015): Central visual pathways in glaucoma: Evidence for distal mechanisms of neuronal self-repair. J Neuroophthalmol 35(Suppl 1):S29–S37.

Dai H, Morelli JN, Ai F, Yin D, Hu C, Xu D, Li Y (2012): Resting-state functional MRI: Functional connectivity analysis of the visual cortex in primary open-angle glaucoma patients. Hum Brain Mapp 34:2455–2463.

Dai H, Yin D, Hu C, Morelli JN, Hu S, Yan X, Xu D (2013): Whole-brain voxel-based analysis of diffusion tensor MRI parameters in patients with primary open angle glaucoma and correlation with clinical glaucoma stage. Neuroradiology 55: 233–243.

Damoiseaux JS, Rombouts SA, Barkhof F, Scheltens P, Stam CJ, Smith SM, Beckmann CF (2006): Consistent resting-state networks across healthy subjects. Proc Natl Acad Sci USA 103: 13848–13853.

De Luca M, Beckmann CF, De Stefano N, Matthews PM, Smith SM (2006): fMRI resting state networks define distinct modes of long-distance interactions in the human brain. Neuroimage 29:1359–1367.

Douaud G, Smith S, Jenkinson M, Behrens T, Johansen-Berg H, Vickers J, James S, Voets N, Watkins K, Matthews PM, James A (2007): Anatomically related grey and white matter abnormalities in adolescent-onset schizophrenia. Brain 130: 2375–2386.

El-Rafei A, Engelhorn T, Warntges S, Dorfler A, Hornegger J, Michelson G (2011): A framework for voxel-based morphometric analysis of the optic radiation using diffusion tensor imaging in glaucoma. Magn Reson Imaging 29:1076–1087.

Engelhorn T, Michelson G, Waerntges S, Struffert T, Haider S, Doerfler A (2011): Diffusion tensor imaging detects rarefaction of optic radiation in glaucoma patients. Acad Radiol 18: 764–769.

Engelhorn T, Michelson G, Waerntges S, Hempel S, El-Rafei A, Struffert T, Doerfler A (2012): A new approach to assess intracranial white matter abnormalities in glaucoma patients: Changes of fractional anisotropy detected by 3T diffusion tensor imaging. Acad Radiol 19:485–488.

EuropeanGlaucomaSociety (2008): Terminology and Guidelines for Glaucoma, 3rd ed. Savona: Dogma.

Fazekas F, Chawluk JB, Alavi A, Hurtig HI, Zimmerman RA (1987): MR signal abnormalities at 1.5 T in Alzheimer's dementia and normal aging. AJR Am J Roentgenol 149: 351–356.

Frezzotti P, Giorgio A, Motolese I, De Leucio A, Iester M, Motolese E, Federico A, De Stefano N (2014): Structural and functional brain changes beyond visual system in patients with advanced glaucoma. PLoS One 9:e105931.

Garaci FG, Bolacchi F, Cerulli A, Melis M, Spano A, Cedrone C, Floris R, Simonetti G, Nucci C (2009): Optic nerve and optic radiation neurodegeneration in patients with glaucoma: In vivo analysis with 3-T diffusion-tensor MR imaging. Radiology 252:496–501.

Ghiso JA, Doudevski I, Ritch R, Rostagno AA (2013): Alzheimer's disease and glaucoma: Mechanistic similarities and differences. J Glaucoma 22(Suppl 5):S36–S38.

Golland Y, Golland P, Bentin S, Malach R (2008): Data-driven clustering reveals a fundamental subdivision of the human cortex into two global systems. Neuropsychologia 46:540–553.

Good CD, Johnsrude IS, Ashburner J, Henson RN, Friston KJ, Frackowiak RS (2001): A voxel-based morphometric study of ageing in 465 normal adult human brains. Neuroimage 14: 21–36.

Grill-Spector K, Kourtzi Z, Kanwisher N (2001): The lateral occipital complex and its role in object recognition. Vision Res 41: 1409–1422.

Gupta N, Yucel YH (2007): Glaucoma as a neurodegenerative disease. Curr Opin Ophthalmol 18:110–114.

Gupta N, Ang LC, Noel de Tilly L, Bidaisee L, Yucel YH (2006): Human glaucoma and neural degeneration in intracranial optic nerve, lateral geniculate nucleus, and visual cortex. Br J Ophthalmol 90:674–678.

Hardy J, Revesz T (2012): The spread of neurodegenerative disease. N Engl J Med 366:2126–2128.

Hernowo AT, Boucard CC, Jansonius NM, Hooymans JM, Cornelissen FW (2011): Automated morphometry of the visual pathway in primary open-angle glaucoma. Invest Ophthalmol Vis Sci 52:2758–2766.

Hodapp E, Parrish RK, Andersson DR (1993): Clinical Decision in Glaucoma. St. Louis: C.V. Mosby Company.

Jenkinson M, Beckmann CF, Behrens TE, Woolrich MW, Smith SM (2012): Fsl. Neuroimage 62:782–790.

Jindal V (2013): Glaucoma: An extension of various chronic neurodegenerative disorders. Mol Neurobiol 48:186–189.

Kumar DK, Choi SH, Washicosky KJ, Eimer WA, Tucker S, Ghofrani J, Lefkowitz A, McColl G, Goldstein LE, Tanzi RE, Moir RD (2016): Amyloid-beta peptide protects against microbial infection in mouse and worm models of Alzheimer's disease. Sci Transl Med 8:340ra72.

Lam DY, Kaufman PL, Gabelt BT, To EC, Matsubara JA (2003): Neurochemical correlates of cortical plasticity after unilateral elevated intraocular pressure in a primate model of glaucoma. Invest Ophthalmol Vis Sci 44:2573–2581.

Li C, Cai P, Shi L, Lin Y, Zhang J, Liu S, Xie B, Shi Y, Yang H, Li S, Du H, Wang J (2012): Voxel-based morphometry of the visual-related cortex in primary open angle glaucoma. Curr Eye Res 37:794–802.

Li T, Liu Z, Li J, Tang Z, Xie X, Yang D, Wang N, Tian J, Xian J (2014): Altered amplitude of low-frequency fluctuation in primary open-angle glaucoma: A resting-state FMRI study. Invest Ophthalmol Vis Sci 56:322–329.

Lindner C, Dannlowski U, Walhofer K, Rodiger M, Maisch B, Bauer J, Ohrmann P, Lencer R, Zwitserlood P, Kersting A, Heindel W, Arolt V, Kugel H, Suslow T (2014): Social alienation in schizophrenia patients: Association with insula responsiveness to facial expressions of disgust. PLoS One 9:e85014.

Liu X, Wang S, Zhang X, Wang Z, Tian X, He Y (2014): Abnormal amplitude of low-frequency fluctuations of intrinsic brain activity in Alzheimer's disease. J Alzheimers Dis 40:387–397.

Loitfelder M, Filippi M, Rocca M, Valsasina P, Ropele S, Jehna M, Fuchs S, Schmidt R, Neuper C, Fazekas F, Enzinger C (2012): Abnormalities of resting state functional connectivity are related to sustained attention deficits in MS. PLoS One 7:e42862.

London A, Benhar I, Schwartz M (2013): The retina as a window to the brain-from eye research to CNS disorders. Nat Rev Neurol 9:44–53.

Martinez K, Solana AB, Burgaleta M, Hernandez-Tamames JA, Alvarez-Linera J, Roman FJ, Alfayate E, Privado J, Escorial S, Quiroga MA, Karama S, Bellec P, Colom R (2013): Changes in resting-state functionally connected parietofrontal networks after videogame practice. Hum Brain Mapp 34:3143–3157.

Michelson G, Engelhorn T, Warntges S, El Rafei A, Hornegger J, Doerfler A (2013): DTI parameters of axonal integrity and demyelination of the optic radiation correlate with glaucoma indices. Graefes Arch Clin Exp Ophthalmol 251:243–253.

Murai H, Suzuki Y, Kiyosawa M, Tokumaru AM, Ishii K, Mochizuki M (2013): Positive correlation between the degree of visual field defect and optic radiation damage in glaucoma patients. Jpn J Ophthalmol 57:257–262.

Packard MG, Knowlton BJ (2002): Learning and memory functions of the Basal Ganglia. Annu Rev Neurosci 25:563–593.

Ray K, Mookherjee S (2009): Molecular complexity of primary open angle glaucoma: Current concepts. J Genet 88:451–467.

Rytty R, Nikkinen J, Paavola L, Abou Elseoud A, Moilanen V, Visuri A, Tervonen O, Renton AE, Traynor BJ, Kiviniemi V, Remes AM (2013): GroupICA dual regression analysis of resting state networks in a behavioral variant of frontotemporal dementia. Front Hum Neurosci 7:461.

Smith SM (2002): Fast robust automated brain extraction. Hum Brain Mapp 17:143–155.

Smith SM, Jenkinson M, Woolrich MW, Beckmann CF, Behrens TE, Johansen-Berg H, Bannister PR, De Luca M, Drobnjak I, Flitney DE, Niazy RK, Saunders J, Vickers J, Zhang Y, De Stefano N, Brady JM, Matthews PM (2004): Advances in functional and structural MR image analysis and implementation as FSL. Neuroimage 23(Suppl 1):S208–S219.

Smith SM, Jenkinson M, Johansen-Berg H, Rueckert D, Nichols TE, Mackay CE, Watkins KE, Ciccarelli O, Cader MZ, Matthews PM, Behrens TE (2006): Tract-based spatial statistics: Voxelwise analysis of multi-subject diffusion data. Neuroimage 31:1487–1505.

Song Y, Mu K, Wang J, Lin F, Chen Z, Yan X, Hao Y, Zhu W, Zhang H (2014): Altered spontaneous brain activity in primary open angle glaucoma: A resting-state functional magnetic resonance imaging study. PLoS One 9:e89493.

Vincent JL, Kahn I, Snyder AZ, Raichle ME, Buckner RL (2008): Evidence for a frontoparietal control system revealed by intrinsic functional connectivity. J Neurophysiol 100:3328–3342.

Wang Z, Yan C, Zhao C, Qi Z, Zhou W, Lu J, He Y, Li K (2011): Spatial patterns of intrinsic brain activity in mild cognitive impairment and Alzheimer's disease: A resting-state functional MRI study. Hum Brain Mapp 32:1720–1740.

Wang MY, Wu K, Xu JM, Dai J, Qin W, Liu J, Tian J, Shi D (2013): Quantitative 3-T diffusion tensor imaging in detecting optic nerve degeneration in patients with glaucoma: Association with retinal nerve fiber layer thickness and clinical severity. Neuroradiology 55:493–498.

Ward NJ, Ho KW, Lambert WS, Weitlauf C, Calkins DJ (2014): Absence of transient receptor potential vanilloid-1 accelerates stress-induced axonopathy in the optic projection. J Neurosci 34:3161–3170.

Wicker B, Keysers C, Plailly J, Royet JP, Gallese V, Rizzolatti G (2003): Both of us disgusted in My insula: The common neural basis of seeing and feeling disgust. Neuron 40:655–664.

Wostyn P, Van Dam D, Audenaert K, Killer HE, De Deyn PP, De Groot V (2015): A new glaucoma hypothesis: A role of glymphatic system dysfunction. Fluids Barriers CNS 12:16.

Zhang Y, Brady M, Smith S (2001): Segmentation of brain MR images through a hidden Markov random field model and the expectation-maximization algorithm. IEEE Trans Med Imaging 20:45–57.

Zhang YQ, Li J, Xu L, Zhang L, Wang ZC, Yang H, Chen CX, Wu XS, Jonas JB (2012): Anterior visual pathway assessment by magnetic resonance imaging in normal-pressure glaucoma. Acta Ophthalmol 90:e295–e302.

Zhang Y, Chen X, Wen G, Wu G, Zhang X (2013): Proton magnetic resonance spectroscopy ((1)H-MRS) reveals geniculocalcarine and striate area degeneration in primary glaucoma. PLoS One 8:e73197.

Zikou AK, Kitsos G, Tzarouchi LC, Astrakas L, Alexiou GA, Argyropoulou MI (2012): Voxel-based morphometry and diffusion tensor imaging of the optic pathway in primary open-angle glaucoma: A preliminary study. AJNR Am J Neuroradiol 33:128–134.